Journal of Energy Storage 89 (2024) 111729

Contents lists available at ScienceDirect

Journal of Energy Storage

journal homepage: www.elsevier.com/locate/est

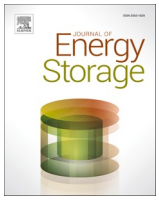

Research papers

Evaluation of volcanic ash as a low-cost high-temperature thermal energy storage material for concentrated solar power

Marc Majó, Adela Svobodova-Sedlackova, A. Inés Fernández, Alejandro Calderón, Camila Barreneche *

Departament de Ciència de Materials i Química Física, Universitat de Barcelona, C/Martí i Franqués 1, 08028 Barcelona, Spain

ARTICLE INFO

Keywords:
Concentrate Solar Power (CSP)
Thermal Energy Storage (TES)
Molten salts
Solid particle storage
High-temperature storage
Alternative materials

ABSTRACT

The integration of renewable energy sources is facilitated by TES because it enables the storage and release of excess clean energy, which improves grid stability. In concentrating solar power plants (CSP), solar molten salt is frequently used since it has some advantages such as good thermal properties. However, certain challenges, such as molten salt corrosion, salt solidification, and high production costs, must be carefully considered. An alternative approach gaining attention involves the use of solid ceramic materials capable of withstanding high temperatures as a potential TES medium without the molten salt drawbacks. Elevating the operating temperature of power conversion processes while concurrently reducing capital costs is a strategic means to enhance the competitiveness of these innovative power plants. This study explores the potential of volcanic ash, a low-cost naturally occurring ceramic material, for TES. The evaluation revealed high-temperature stability up to 750 °C, slight mass gain but stable over time, elevated solar absorption, and excellent thermal and chemical stability, even in the presence of molten salts.

1. Introduction

A potential answer to the world's energy issue of balancing energy supply and demand is thermal energy storage (TES). During times of low demand, excess clean energy can be stored and released later using TES systems [1]. The International Energy Agency (IEA) [2] claims that TES can increase grid stability and dependability while also being a cost-effective solution to integrate renewable energy sources like solar and wind power. By reducing the usage of thermal power plants that burn fossil fuels to meet peak demand, TES can also contribute to producing lower greenhouse gas emissions.

A solar power generation system, known as a Concentrated Solar Power (CSP) tower plant, incorporates an energy storage system that utilizes molten salts as both Thermal Energy Storage (TES) and heat transfer fluid (HTF). This system uses heliostat mirrors to concentrate solar energy, heating the HTF, which is then employed to generate electricity by transferring the heat into a power block through a heat exchanger. The heated molten salts can be stored for several hours, enabling continuous electricity production even during periods without sunlight, thereby avoiding the "duck effect" [3,4]. Typically, sodium nitrate and potassium nitrate, which have high heat capacities and can be heated to temperatures over 400 °C, are combined to create one of the molten salts used in CSP plants, known as solar salt (60:40 $NaNO_3$:KNO_3) [5,6]. The solar tower plant is recognized as one of the most advanced and established configurations in the field of Concentrated Solar Power (CSP) for large-scale solar power generation and storage. It is currently utilized in several large-scale power plants worldwide, such as the Crescent Dunes in Nevada, USA, and the Gemasolar Thermosolar Plant in Seville, Spain, boasting thermal storage capacities of up to 10 and 15 h, respectively [7,8]. In many nations, including China, the United Arab Emirates, Morocco, South Africa, the United States, and Chile, numerous projects are now under construction, and more tower CSP plants with heat storage systems are anticipated in the upcoming years. Additionally, several projects using different solar power technology will be finished in the upcoming years [9].

Solid-state thermal storage utilizing concrete or solid particles [10] is being studied as TES media. Some of these solid materials are affordable and can potentially lower the amount of solar salt needed in the plant and thus, lower the capital expense of CSP utilities [11]. These materials are suitable for use in CSP due to their high thermal energy storage density, which is comparable to molten salts [12]. Moreover, these materials can withstand higher temperatures, rendering them suitable

* Corresponding author.
E-mail address: c.barreneche@ub.edu (C. Barreneche).

https://doi.org/10.1016/j.est.2024.111729
Received 18 January 2024; Received in revised form 21 March 2024; Accepted 17 April 2024
Available online 30 April 2024

for use in CSP systems. Although sensible solid thermal energy storage systems have a lower energy density in terms of kWh/m^3 compared to other liquids, latent processes, or thermochemical processes, they are currently more extensively studied and commercially developed [10]. Despite of this, solid particles are being considered as a good candidate to work as a HTF and TES material for the next-generation CSP plants. Increasing the operational temperature can result in a higher thermodynamic efficiency [13]. Furthermore, using low-cost ceramic particles instead of traditional molten salts can reduce capital and operational costs of the plant.

By employing high-temperature particles, it is possible to raise the maximum storage temperature, leading to an increase in the thermal-to-electric efficiency of power cycles. Additionally, it allows for the utilization of other HTF to achieve higher cycle efficiency at elevated temperatures, such as supercritical CO_2. The implementation of the supercritical CO_2 process, characterized by simpler machinery and a compact size compared to other steam power cycles, has the potential to reduce costs associated with system installation, maintenance, and operation [14]. Currently, there are ongoing investigations and tests on particle solar receivers, which are used to capture solar radiation from the heliostat field. Unlike conventional receivers, particle receivers use solid particles that are heated as they fall through a beam of concentrated sunlight [15]. It will be possible to increase the temperature of the heat-transfer media to over 1000 °C by using ceramic particle materials and this particle receiver technology. Solid particle in CSP technology offers a potential solution to the challenges associated with the current use of molten salts. Furthermore, the enhanced performance resulting from energy conversion at higher temperatures and the considerably lower cost of these particulate ceramics, particularly when obtained from alternative or natural sources, have the potential to significantly enhance the competitiveness of concentrated solar power plants [16].

When searching for natural rocks capable of withstanding high temperatures for multiple cycles or having good contact with different HTFs, numerous rock types have been investigated [17]. Several mineral groups from different families of igneous, metamorphic, or sedimentary rock have shown good stability at high temperatures over a considerable number of cycles [18]. High temperature stability, high density, and high heat capacity are some of the main properties required to be suitable as a thermal storage material. Another necessary property in the case of particle solar receivers is having high solar absorptance [19]. Taking all these factors into consideration, an extrusive igneous rock type such as volcanic rock can be of interest as a low-cost natural material for use in concentrated solar power plants. After the volcanic eruption on the island of La Palma, Canary Islands, Spain, that took place in 2021, it was estimated that the volcanic activity expelled around 200 Mm^3 of total pyroclastic in different flows [20]. This large amount of rock waste was scattered across the island, making life difficult for many people. After the 85 days of eruption, the rehabilitation of areas led to the accumulation of enormous quantities of volcanic rock waste, most of which are destined for civil engineering applications. However, due to the favourable temperature properties present in igneous rocks [18], this material remains of great interest for studying applications at high temperatures such as TES. A TES tank with volcanic rock and air as HTF is already in operation since 2019 in the north of Germany. The single 1.5 MW TES tank operated by Siemens Gamesa, heat up the particles up to 800 °C and when is fully charged, the turbine can generate electricity for 24 h [21].

A complete evaluation of volcanic ash particles was conducted to provide insights into the materials aspect of high-temperature TES. To achieve this, key properties necessary for the TES material were studied for two purposes: (1) Utilizing volcanic ash as TES material in direct contact with molten salts. This approach is considered feasible as the technology involving the receiver and power block is well-established in many existing CSP plants and planned for future projects [9]. While this concept reduces the use of molten salts and associated challenges, it does not eliminate them entirely. Conversely, (2) volcanic ash is also being considered for a Solid Particle Solar Receiver (SPSR) concept, where the material captures heat in the receiver and transfers it to the TES tank. Properties such as solar absorptance, high temperature stability, and mechanical stability need to be considered for this strategy. Although not as extensively researched as the conventional molten salt receiver, the benefits associated with this concept, such as higher operational temperatures contributing to better thermodynamic performance [13], fewer compatibility issues, and reduced capital costs [15], make it an interesting area for exploration.

A comprehensive assessment of volcanic ash for high-temperature TES is the primary focus of the current study. A thermal cycling test, ranging from 250 °C to 750 °C conducted 1000 times, is aimed at pushing the material's integrity to the limit and detecting any changes. Additionally, a compatibility test with molten salts has been completed at 400 °C for 500 h, followed by a chemical and thermal comparison of the molten salt to identify any alterations in its structure and properties. Finally, optical and thermo-mechanical tests are conducted on the material to evaluate all properties for integrating this natural waste in a packed-bed configuration with a HTF in contact with the materials.

2. Materials and methodology

2.1. Materials

The volcanic ash obtained for this research was collected and provided by members of the Institute for Environmental Studies and Natural Resources (I-UNAT) at the University of Las Palmas de Gran Canaria. They gathered samples near El Paso village, situated on the western flank of La Palma island's Cumbre Vieja rift zone in the Canary Islands, Spain.

For a compatibility test with molten salts, Solar Salt was used since it is the most common commercial thermal fluid used in concentrating solar power plants. Solar Salt mixture consists of sodium nitrate and potassium nitrate (60:40 wt% respectively). Both compounds were obtained from the company Merck ACS reagent grade with a purity >99.5 %. The Solar Salt mixtures were obtained with the preparation of 60:40 weight percentage of sodium nitrate and potassium nitrate, respectively.

2.2. Thermal and compatibility tests

2.2.1. Thermal cycling test

To carry out this experiment, the thermal cycling test was conducted by means of a specialized Carbolite-gero equipment, designed for the Birmingham Centre for Energy Storage (BCES). This involves an automated cycling mechanism that transfers the sample into a high-temperature zone and maintains it at the desired temperature for a specific duration. Subsequently, the sample is relocated to a low-temperature area for cooling. This cycle is repeated as many times as necessary.

For the cycling test, a small round tablet made of volcanic ash was fabricated using an automated press and a specific mould. The resulting round tablet sample measured 3.81 mm in thickness and 12.7 mm in diameter. The tablet underwent 1000 cycles, alternating between temperatures of 250 °C and 750 °C in an air atmosphere. Each complete cycle lasted 22 min, comprising 10 min of heating inside the furnace and 12 min in the lower-temperature zone using a fan for controlled cooling.

2.2.2. Compatibility test with molten salts

The compatibility test of Solar Salt and the volcanic ashes were carried out under air atmosphere with an alumina crucible in an open standard furnace. The test conditions consisted of an isotherm at 400 °C for 500 h and the mixture of the materials was carried out at around 300 °C to avoid bubbling and the decomposition of some solids. Then a heating ramp of 10 °C/min was applied until 400 °C. The choice of the test temperature was based on the expected average operating temperature of the materials in the intended application. After the test, the

materials were separated with a metallic sieve with a mesh diameter of 0.5 mm and then dissolved in water and separated with a filter paper with a retention size of 15–20 μm to separate the smaller particles. Hence, after evaporating the water it only remains the solid particles and a sample of solar salt that has been in contact with that solid. Finally, the two samples of solar salt exposed at temperature were analysed. Solar salt alone and the sample of solar salt in contact with the solid, both were evaluated for the presence of [NO_2^-] in order to evaluate the degradation of the salt.

2.3. Characterization techniques

2.3.1. Physical evaluation

A physical characterization was performed by determining the following aspects: the real density through the helium pycnometer (Accu-Pyc 1330) and the particle size distribution (PSD) with a laser diffraction particle size analyser (Beckman Coulter LSTM 13320), where the results were analysed using Fraunhofer mathematical model, which is used for opaque particles bigger than 30 μm. Also, SEM images were conclusive to evaluate the surface of the particles. A Hitachi TM3030 scanning electron microscope was used to obtain the surface and EDS images before and after the thermal exposure.

2.3.2. Chemical evaluation

Chemical analysis consists of a major compounds' evaluation through X-Ray Fluorescence, XRF (Panalytical Philips PW 2400). Then a crystalline phase's determination of the materials had been completed with a powder X-Ray diffraction, XRD, equipment (Bruker D8). A comparison of XRD patterns was also made with the different samples before and after the thermal cycle. Conversely, to check the compatibility with Solar Salt, a UV–Vis spectroscopy evaluation was carried out to quantify the [NO_2^-] concentration in the Solar Salt after the thermal exposure with the volcanic ashes. A UV–Vis spectrophotometer Shimadzu UV-1280 was used for the characterization. Since the [NO_2^-] formation is the first reaction that will lead to a degradation of the salt [22], a quantification of the [NO_2^-] formation is a key indicator of Solar Salt/solid compatibility. To quantify the [NO_2^-] concentration in the pure Solar Salt and the Sola Salt that has been in contact with volcanic ash after thermal exposure, a calibration should be completed with different [NO_2^-] concentrations. The indirect method used to quantify the nitrite concentration was already used by Svobodova-Sedlackova, et al. [23] for the determination of [NO_2^-] in $NaNO_3$ mixtures with nanoparticles. The UV–Vis absorption spectra were performed with $NaNO_3$/$NaNO_2$ mixtures at 0.3 M for a $NaNO_2$ concentration of 1 wt%, 2 wt%, 3 wt%, 4 wt%, and 5 wt%. The absorption peaks for [NO_2^-] and [NO_3^-] were detected at 354 nm and 300 nm, respectively. Fig. 1(a) depicts the increase of nitrite peak intensity with $NaNO_2$ concentration. Also, the absorbance of nitrite peaks as a function of concentration, Fig. 1(b), shows a linear trend with $R = 0.998$, intersection $= 0.0024 \pm 0.0062$ and slope $= 0.0722 \pm 0.0019$, with a good accuracy, $\sigma = \pm 0.0059$.

2.3.3. Thermal evaluation

A thermogravimetric analysis (TGA) was conducted up to 750 °C to evaluate changes in the solid particles. Also, a differential scanning calorimetry (DSC) analysis was carried out in a single sample through a simultaneous thermal analysis, STA, (STA 449 F3 Jupiter Netzsch) equipment at the University of Birmingham. Both analyses were conducted in air atmosphere with a heating ramp of 10 °C/min in a powder form and a mass of around 50 mg in a Pt crucible. The specific heat capacity of the sample at 300 °C and 750 °C under air atmosphere was calculated following the methodology for specific heat capacity determination of materials for thermal energy storage described by Ferrer et al. [24].

Thermal conductivity of the volcanic ash sample was calculated with a Laser Flash, LFA, (LFA 427 Netzsch) at the University of Birmingham. A round tablet of 2 cm of diameter and 1.3 mm of thickness was created to conduct the evaluation. The thermal diffusivity of the sample will be determined by the equipment as expressed in Eq. (1), where I is the sample thickness and $t_{0.5}$ is the time at 50 % of the temperature increase. Then, thermal conductivity of the sample can be calculated with the equation expressed in Eq. (2), where λ is the thermal conductivity, a is the thermal diffusivity obtained experimentally, C_p the heat capacity of the material and ρ the bulk density of the sample. This principle was obtained from the LFA equipment manual for thermal conductivity determination.

$$a = 0.1388\frac{I^2}{t_{0.5}} \tag{1}$$

$$\lambda = a \cdot C_p \cdot \rho \tag{2}$$

2.3.4. Optical evaluation

The calculation of solar absorption was done with a UV–Vis spectrophotometer with an integrating sphere. The test covered from 250 nm to 2500 nm with a step of 5 nm. The sample-holder was built with a sapphire window and then, with an optical model for window corrections, the influence of the sapphire glass was eliminated. The correction method used assumed a flat angular behaviour, where the simplest approach is to suppose that transmittance (τ_w) and reflectance (ρ_w) of the sapphire window is approximately the same that window transmittance ($\{\tau_w\}$) and reflectance ($\{\rho_w\}$) averaged over the reflection/diffusion angle. So, the reflectance of the solids (R_s) can be calculated as Eq. (3) [25]:

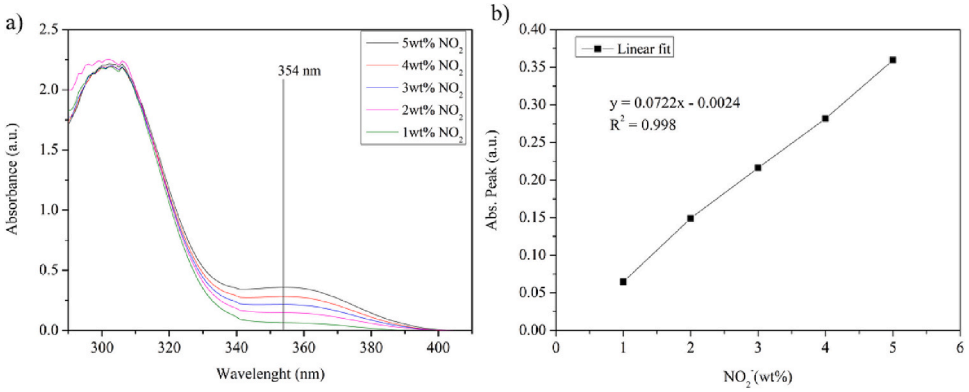

Fig. 1. UV–Vis spectra of 0.3 M $NaNO_3$-$NaNO_2$ solution. a) Evolution of nitrite peak with the concentration of $NaNO_2$ {1 wt%, 2 wt%, 3 wt%, 4 wt%, 5 wt%}and, b) linear relation of light absorption and the concentration of nitrites at a wavelength of 354 nm.

$$R_s = \frac{\rho_{w,s} - \rho_w}{\tau_w^2 + \rho_w(\rho_{w,s} - \rho_w)} \quad (3)$$

where ($\rho_{w,s}$) is the overall hemispherical reflectance spectrum of the specimen measured through the window. Once the absorbance measurements were done, a trapezoidal integration was performed and weighted concerning the solar spectrum AM 1.5 to obtain the solar absorbance value for the whole range (250–2500 nm) [26].

2.3.5. Mechanical testing

A Thermo-Mechanical Analyser (TMA 450, TA Instruments) was used to obtain the coefficient of thermal expansion (CTE) for different temperature ranges of the volcanic ash sample. The total temperature range extended from 50 to 750 °C with a heating rate of 5 °C/min, using an expansion probe and a tablet of 2 cm of diameter and 1.3 mm of thickness. The temperature intervals chosen for CTE determination were from 50 °C to 275 °C, from 275 °C to 500 °C, and from 500 °C up to 725 °C.

3. Results

3.1. Materials and samples

The material under study is presented in Fig. 2. The volcanic ash material as received, Fig. 2(a), the alumina crucibles used for the compatibility between the volcanic ash and Solar Salt, Fig. 2(b), the round tablet of volcanic ash for the thermal cycling test before (Fig. 2(c)) and, after the cycling test, Fig. 1(d).

3.2. Physical evaluation

The real density of volcanic ash sample was evaluated as received in dust form with a helium pycnometer. The obtained real density was 2.41 ± 0.01 g/cm^3. Also, a tablet with of 3.81 mm in thickness, 12.7 mm of diameter and a mass of 0.99 g, was created to conduct the thermal cycling evaluation. The bulk density variation of the tablet before and after the cycling are reported in Table 1.

The PSD evaluation showed a normal distribution in volume percentage (vol%) of particles with a d_{90} of 250 μm, Fig. 3. However, a large number of fine particles were detected. 99.65 % of the particles are below 100 μm and only 0.35 % of the particles are between 100 μm and 600 μm.

In the SEM images presented in Fig. 4, it can be seen the shape and roughness of the volcanic ash particles after a first sieving to avoid the excess of fines. Also, an EDS elemental quantification was done with some particles to identify some inclusions observed on the surface of the particles. The surface of the particles has been observed before and after the thermal cycling. In Fig. 4(a), it can be observed the average particle shape, a detailed image of a particle and an EDS elemental identification of the volcanic ash sample as received. Fig. 4(b), shows the SEM images after the 1000 cycles between 250 °C and 750 °C. At first sight, we can notice some cracks in the surface of many particles, a detailed view of the crack is presented at the same figure. This is probably due to the thermal shock experimented during the cycles. The thermal losses associated with a thermal front featuring high temperature differences will be significant due to the dissipation process, potentially affecting the mechanical integrity of the solids. However, while the thermal shock effect during operation in a cycling mode could be mitigated, it may still be present during the initial phases [27]. Additionally, various particle agglomerations are observed around the larger particles. This agglomeration of aggregates may be attributed to some sintering process at high temperatures.

Table 1
Bulk density of volcanic ash before and after thermal cycling between 300 °C and 750 °C for 1000 cycles.

	As received	After 1000 cycles
Bulk density (g/cm^3)	2.06 ± 0.02	2.02 ± 0.02

3.3. Chemical evaluation

As evaluated by J. Mañosa et al. [28], the volcanic ash are alkaline mafic rocks classified as basanites with similar compositions to those reported on lavas of the 2021 Tajogaite eruption [29] and, with a comparable chemical composition with the volcanic ash collected from other mafic alkaline volcanic eruptions worldwide.

The evaluation through XRF can be observed in Table 2 where the percentage of major compounds in a sample of volcanic ash are presented. It can be observed a significant presence of SiO_2, as well as Fe_2O_3, Al_2O_3 and CaO in a smaller but significant percentage. In a lesser percentage, MgO, TiO_2, Na_2O, K_2O, P_2O_5 and MnO have also been detected.

XRD diffractograms before and after thermal cycling of the volcanic ash are shown in Fig. 5. Different families of silicates, such as diopside ($(Ca,Mg)Si_2O_6$), anorthite ($(Ca, Al_2)Si_2O_8$), and olivine ($Mg_{1.727}Fe_{0.273}SiO_4$) has been identified. In addition, a relevant amorphous content can be expected due to the fast cooling that the material experimented during the eruption. In the sample before the thermal cycling, Fig. 5(a), Diopside and anorthite minerals has the majoritarian crystalline phases that conforms the volcanic ash. Minor crystallographic phases as metallic oxides such magnetite (Fe_3O_4) and titanomagnetite ($Fe_{2.25}Ti_{0.75}O_4$) have been also detected. After the cycling test, Fig. 5(b), a second crystallographic determination was done to evaluate the possible changes in the sample. The associated peaks to magnetite were transformed into hematite (Fe_2O_3), in accordance with the reported by [30] in this temperature range and the reddish color observed after the thermal cycling, which is characteristic to the mineral hematite (Fig. 2(d)). As a result, a slight increase in mass is anticipated due to the oxidation of iron compounds. This is validated by the TGA analysis presented in Table 4, indicating a noticeable mass gain during the initial thermal exposure. Otherwise, the peaks associated with the

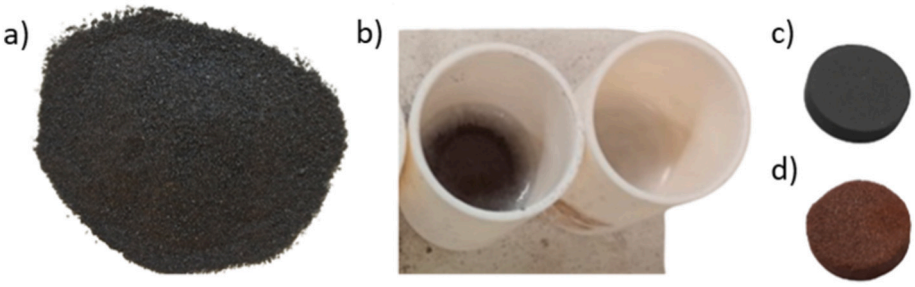

Fig. 2. a) Sample of volcanic ash as received, b) alumina crucibles with molten Solar Salt (right) and molten Solar Salt in contact with volcanic ash (left), c) tablet of volcanic ash created for the cycling evaluation before the cycling and, d) after 1000 cycles between 250 °C–750 °C.

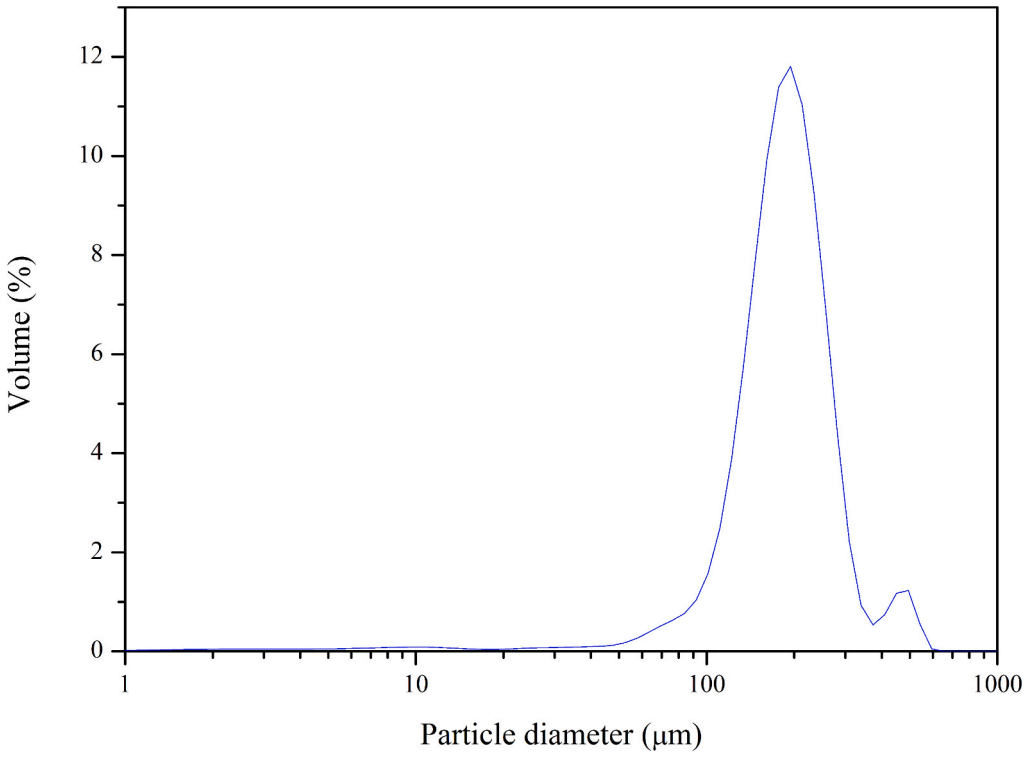

Fig. 3. PSD distribution of volcanic ashes as received expressed in a volume percentage (vol%).

titanomagnetite phase remain unaltered in our sample, suggesting a lack of observable modifications. According to the study documented in [31], titanomagnetite has the potential to transform, oxidizing into ilmenite ($FeTiO_3$) and further progressing from ilmenite to rutile (TiO_2) at temperatures below 850 °C. Despite the presence of a small amount of titanomagnetite in our sample, specific alterations related to these transitions are not prominently evident. While the temperature range in our testing methodology might initiate these reactions, our findings have not detected such transformations.

With the linear equation presented in Fig. 1(b), is it possible to quantify the nitrite percentage of the Solar Salt and Solar Salt in contact with volcanic ash samples. Results of UV–Vis spectra of 0.3 M solution for Solar Salt alone and Solar Salt in contact with volcanic ash (after the thermal exposure) are presented in Fig. 6. Also, the UV–Vis spectra calculation results of $[NO_2^-]$ concentration are shown in Table 3. The calculations of $[NO_2^-]$ concentration at the main absorption peak of $[NO_2^-]$ are certainly similar, however a slight difference in nitrite concentration can be spotted.

After the thermal cycling, the Solar Salt sample in contact with volcanic ash shows an increase in nitrite concentration of over 0.48 %, compared to the 0.17 % of the pure Solar Salt sample. Therefore, the results indicate that the presence of volcanic ash in Solar Salt tends to influence the formation of nitrites, serving as a catalyst for the decomposition reaction. Although nitrite formation naturally occurs due to the influence of oxygen within the specified temperature range [32], the presence of certain compounds in the volcanic ash sample can accelerate the reduction of nitrates to nitrites.

3.4. Thermal evaluation

Thermal stability in terms of mass variation (%), specific heat capacity, thermal conductivity and thermal diffusivity of volcanic ash are reported in Table 4. The thermal evaluation was done at 300 °C and 750 °C to evaluate the stability in this temperature range. Also, values at the first and second temperature cycle and after the thermal cycling test, were determined. An increase in mass was detected after the first cycle, likely due to the oxidation of iron compounds. Additionally, a reddish color appeared in the sample after thermal exposure. This mass variation remained constant throughout subsequent thermal cycles. The specific heat capacity experienced a slight reduction after the cycles; however, the variation is not significant and falls within the measurement error range. Similarly, thermal conductivity increased with temperature compared to values before thermal exposure, correlating with the specific heat capacity. The calculated thermal diffusivity showed an increase from values before to after the treatment, also dependent on temperature.

Related to the compatibility of the volcanic ash and molten salts, a thermal evaluation of Solar Salt as received and Solar Salt that has been in contact with volcanic ashes for 500 h at 400 °C, are presented in Table 5. A slight change in specific heat capacity is detected in the sample of Solar Salt in contact with volcanic ash. However, the variation of all thermal properties and melting point of the sample remained almost invariant after the compatibility test. The decrease in the enthalpy heat of fusion and the melting point of Solar Salt with increasing nitrite concentration has been reported in several articles [33–35]. However, the nitrite concentration calculated in the chemical evaluation of the salts does not show a significant increase of nitrites in the solar salt sample in contact with volcanic ashes.

3.5. Optical evaluation

The ratio of solar absorptance is the fraction of the total incident solar radiation that is absorbed by the material, with the remainder being reflected. In Fig. 7, the solar absorptance detected with the sapphire window correction applied is presented. The averaged solar spectrum absorptance of the volcanic ash sample was 85.19 %. This value was obtained by means of a trapezoidal integration of all solar spectrum wavelength and weighted following the solar spectrum AM 1.5. The obtained value aligns with similar studies on ceramic particles intended for a direct-use in CSP plants, showing solar absorptance ranging between 85 and 90 % [26]. Nevertheless, a comprehensive, long-term characterization is necessary to assess any changes in

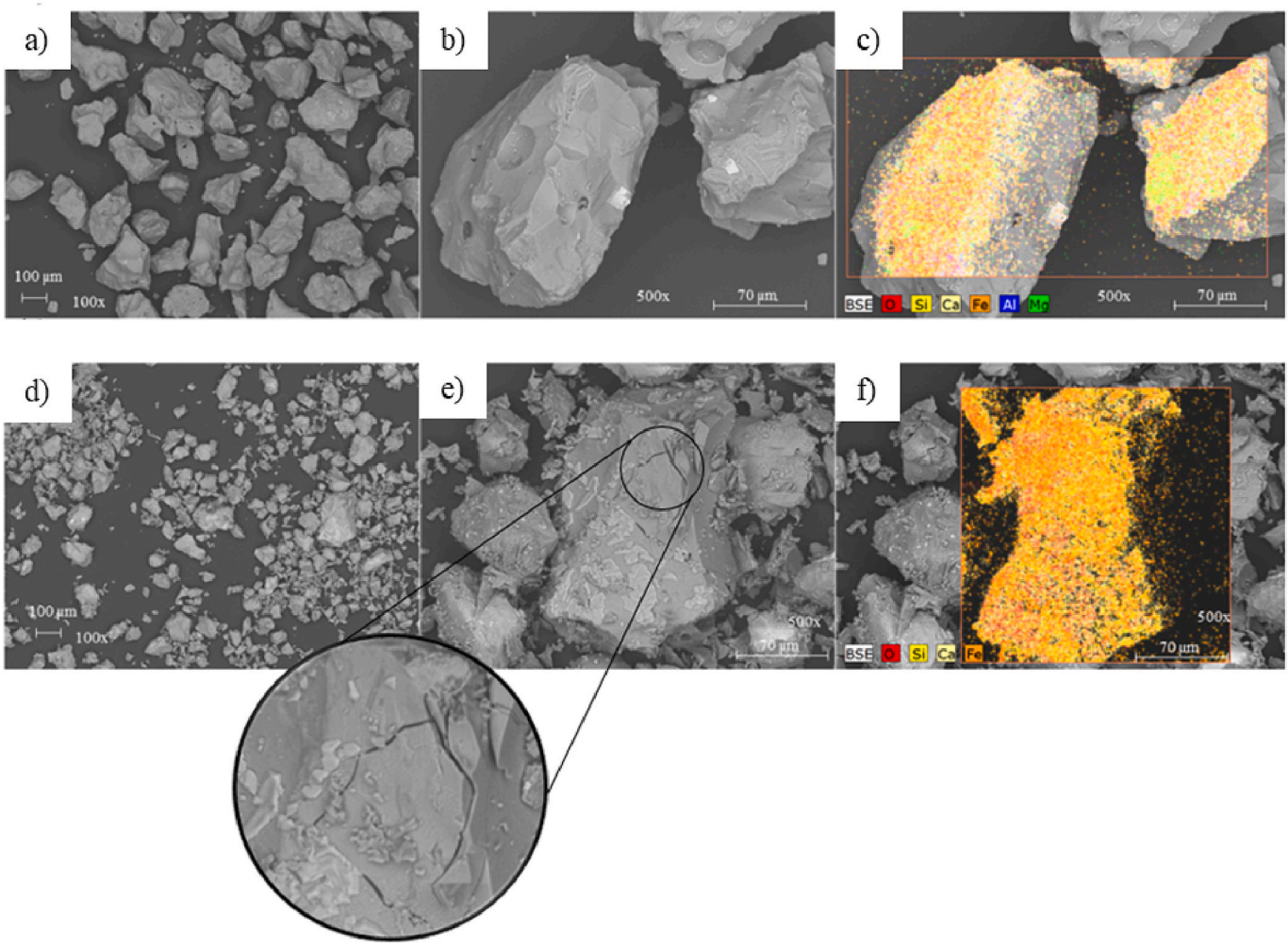

Fig. 4. SEM and EDS images of: a) volcanic ash as received at 100× and b) 500× of magnitude with c) EDS analysis, and, d) volcanic ash after thermal cycling test: 1000 cycles between 250 °C and 750 °C, at 100×, e) 500× and f) EDS analysis.

Table 2
Main chemical composition of volcanic ash sample determined by XRF.

Major compounds	SiO_2	Fe_2O_3	Al_2O_3	CaO	MgO	TiO_2	Na_2O	K_2O	P_2O_5	MnO
wt%	43.7	13.6	13.2	11.6	8.5	3.7	3.3	1.4	0.8	0.2

absorptance over time.

3.6. Mechanical testing

The CTE of the volcanic ash and the percentage of change in all temperature ranges selected are presented in Table 6. Also, a comparison with different materials typically found in TES tank components is reported. The temperature variation in all intervals was 225 °C, and the percentage of change and CTE increases with temperature. It's noticeable that the CTE of volcanic ash is closer to that of Inconel 600, particularly at high temperatures, but significantly different from the values of AISI 347 stainless steel. To prevent potential structural issues in the tank over multiple cycles, the CTE values of the metal components should closely align with those of the ceramic particles. Considering these findings, the utilization of Inconel 600 seems more suitable for applications involving solid particle materials.

3.7. Comparative analysis of the proposed TES material: Solar salt and commercial solid particles

The utilization of volcanic ash as a TESM while employing solar salt as the HTF could offer economic, environmental, and long-term stability benefits. When comparing the energy density calculated of volcanic ash (2.28 J/cm^3) with the average energy density of solar salt at 400 °C (2.81 J/cm^3), it is observed that replacing solar salt with volcanic ash to achieve the same storage capacity would require a greater amount of material in the tank. However, the degradation of solar salt with temperature and the compatibility issues with other elements in the plant, will be avoided. This substitution would mitigate the chemical changes in solar salt with temperature [22], thus ensuring long-term stability. The degradation of solar salt due to temperature leads to a reduction in its specific heat capacity through the formation of [NO_2^-]. Consequently, implementing a packed-bed configuration with volcanic ash could not only benefit long-term stability but also lead to economic improvement due to the low cost of volcanic ash and environmental benefits by repurposing this waste material.

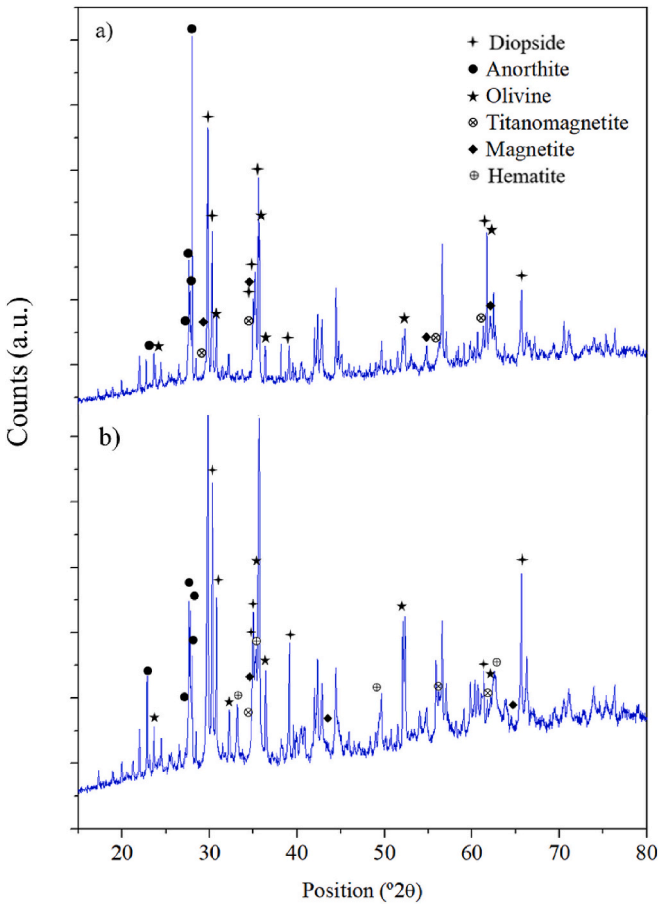

Fig. 5. XRD peak identification and comparison of volcanic ash a) after thermal cycling and b) before thermal cycling of 1000 cycles between 250 °C and 750 °C.

In contrast, the SPSR currently under testing employ sintered ceramic materials possessing ideal characteristics in terms of morphology, chemical, and thermal stability. Utilizing low-cost, thermally stable, and chemically inert ceramic could enhance the competitiveness of these plants by reducing capital costs, especially given the high cost associated with current solid particle materials [38].

Table 3
UV–Vis spectra calculation results of [NO_2^-] presence in solar salt samples.

Samples	Abs. peak at 354 nm (a.u.)	Calculation of [NO_2^-] concentration in the sample (wt%)
Solar salt	0.0103 ± 0.0002	0.175 ± 0.002
Solar salt/ volcanic ash	0.0322 ± 0.0002	0.479 ± 0.002

Table 4
Thermal characterization of volcanic ash. Thermal stability, specific heat capacity, thermal conductivity and thermal diffusivity at 1st, 2nd and 1000 thermal cycles.

Volcanic ash	1st cycle	2nd cycle	1000 cycles
Mass variation (%)	0.57	0.03	0.03
Specific heat capacity at 300 °C (J/g·°C)	0.95 ± 0.02	0.94 ± 0.03	0.90 ± 0.01
Specific heat capacity at 750 °C (J/g·°C)	1.13 ± 0.04	1.20 ± 0.05	1.01 ± 0.04
Thermal conductivity at 300 °C (W/m·°C)	0.36 ± 0.01	–	0.58 ± 0.01
Thermal conductivity at 750 °C (W/m·°C)	0.43 ± 0.01	–	0.61 ± 0.02
Thermal diffusivity at 300 °C (mm^2/s)	0.18 ± 0.01	–	0.31 ± 0.01
Thermal diffusivity at 750 °C (mm^2/s)	0.17 ± 0.01	–	0.29 ± 0.02

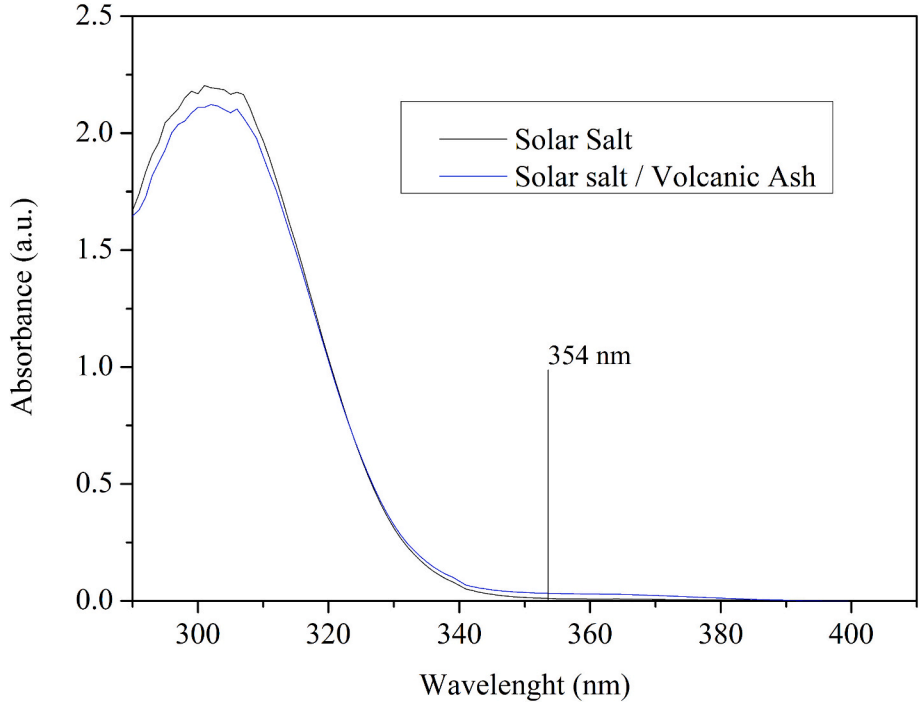

Fig. 6. UV–Vis spectra of 0.3 M solution for Solar Salt and Solar Salt/volcanic ash combination.

Table 5
Specific heat capacity, enthalpy heat of fusion and melting point of solar salt at initial conditions and solar salt and solar salt in contact with volcanic ash after thermal contact at 400 °C for 500 h.

Solar salt in contact with volcanic ash	C_p, 400 °C (J/g·°C)	ΔH_{fus} (J/g)	Melting point (°C)
Solar salt	1.54 ± 0.01	111.24 ± 0.01	226.01 ± 0.01
Solar salt + volcanic ash	1.51 ± 0.01	110.69 ± 0.01	223.60 ± 0.01
Solar salt initial	1.56 ± 0.01	113.60 ± 0.01	227.75 ± 0.01

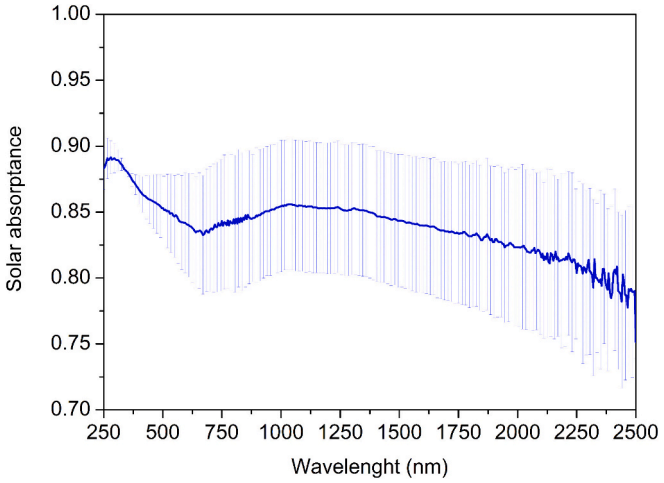

Fig. 7. Solar absorptance results of volcanic ashes in all solar spectrum from 250 nm to 2500 nm.

Table 6
CTE at different temperature ranges of volcanic ashes and its percentage of change in the same temperature range. CTE of stainless steel AISI 347 and Inconel 600 are also reported.

Volcanic ash	CTE (10^{-6}·°C^{-1})	Change (%)	CTE (10^{-6}·°C^{-1}) of AISI 347 [36]	CTE (10^{-6}·°C^{-1}) of Inconel 600 [37]
From 50 °C to 275 °C	8.99 ± 0.90	0.15	17.27	12.30
From 275 °C to 500 °C	12.59 ± 0.19	0.19	19.40	13.95
From 500 °C to 725 °C	15.24 ± 2.95	0.26	20.76	15.65

4. Conclusion

A comprehensive assessment investigated volcanic ashes from La Palma Island's 2021 eruption for high-temperature thermal storage up to 750 °C. The ashes exhibited silicate families, including diopside, anorthite, and olivine in XRD evaluation. Thermal cycling retained the structure but oxidized metallic oxides, shifting from magnetite to hematite, causing a 0.54 % mass gain. Optical properties showed 85 % solar absorptance, crucial for open receiver technology. Volcanic ash displayed a thermal expansion similar to metallic alloys in thermal energy storage tanks. SEM images indicated particle cracking and surface formations post-thermal cycling.

Solar salt in contact with volcanic ash showed no unusual nitrite formation, maintaining its thermal properties. UV–Vis spectroscopy quantified nitrites, useful for monitoring solar salt degradation. Nitrite formation marks the initial stage of solar salt degradation, eventually forming alkaline oxides.

Thereby, volcanic ash from La Palma Island has huge potential to be an alternative and sustainable material to be applied as TES field and to explore its potential.

In conclusion, the evaluated volcanic ash exhibits promising properties for high-temperature Thermal Energy Storage (TES) applications, offering cost-effective solutions and potential energy storage savings.

CRediT authorship contribution statement

Marc Majó: Conceptualization, Data curation, Formal analysis, Investigation, Methodology, Writing – original draft. **Adela Svobodova-Sedlackova:** Conceptualization, Data curation, Formal analysis, Methodology, Writing – review & editing. **A. Inés Fernández:** Conceptualization, Data curation, Investigation, Project administration, Resources, Supervision, Writing – review & editing. **Alejandro Calderón:** Resources, Methodology, Investigation, Funding acquisition, Formal analysis, Conceptualization, Data curation. **Camila Barreneche:** Writing – review & editing, Supervision, Project administration, Methodology, Investigation, Funding acquisition, Conceptualization, Formal analysis.

Declaration of competing interest

The authors declare that they have no known competing financial interests or personal relationships that could have appeared to influence the work reported in this paper.

Data availability

Data will be made available on request.

Acknowledgement

This work is part of RTI2018-093849-B-C32, PCI2020-120695-2 and PCI2020-120682-2 projects funded by Ministerio de Ciencia e Innovación - Agencia Estatal de Investigación (MCIN/AEI/10.13039/501100011033) and by the European Union "NextGeneration EU/PRTR", Development and evaluation of novel concepts for LHTES funded by CSO - Israeli Ministry of Energy, 120N663 project funded by TÜBITAK—Scientific and Technological Research Council of Turkey, and 121N737 project funded by TÜBITAK. This work is supported by 100 Foreign Experts Plan of Hebei Province. The authors would like to thank the Catalan Government for the quality accreditation given to their research group DIOPMA (2017 SGR 0118, 2021 SGR 00708). DIOPMA is a certified agent TECNIO in the category of technology developers from the Government of Catalonia.

References

[1] G. Alva, Y. Lin, G. Fang, An overview of thermal energy storage systems, Energy 144 (2018) 341–378, https://doi.org/10.1016/j.energy.2017.12.037.
[2] IEA Publications, World Energy Outlook 2022, Int. Energy Agency, 2022. https://www.iea.org/reports/world-energy-outlook-2022.
[3] A. Calderón, C. Barreneche, C. Prieto, M. Segarra, A.I. Fernández, Concentrating solar power technologies: a bibliometric study of past, present and future trends in concentrating solar power research, Front. Mech. Eng. 7 (2021) 1–22, https://doi.org/10.3389/fmech.2021.682592.
[4] T. Bauer, C. Odenthal, A. Bonk, Molten salt storage for power generation, Chemie-Ingenieur-Technik 93 (2021) 534–546, https://doi.org/10.1002/cite.202000137.
[5] S.S. Mostafavi Tehrani, R.A. Taylor, K. Nithyanandam, A. Shafiei Ghazani, Annual comparative performance and cost analysis of high temperature, sensible thermal energy storage systems integrated with a concentrated solar power plant, Sol. Energy 153 (2017) 153–172, https://doi.org/10.1016/j.solener.2017.05.044.
[6] T. Bauer, N. Pfleger, N. Breidenbach, M. Eck, D. Laing, S. Kaesche, Material aspects of Solar Salt for sensible heat storage, Appl. Energy 111 (2013) 1114–1119, https://doi.org/10.1016/j.apenergy.2013.04.072.

[7] M. Geyer, U. Herrmann, A. Sevilla, J.A. Nebrera, G. Gomez Zamora, Dispatchable solar electricity for summerly peak loads from the solar thermal projects Andasol-1 y Andasol-2. https://www.osti.gov/etdeweb/biblio/20811671, 2006.

[8] N.R. Avezova, A.E. Khaitmukhamedov, A.Y. Usmanov, B.B. Boliyev, Solar thermal power plants in the world: the experience of development and operation, Appl. Sol. Energy 53 (2017) 72–77, https://doi.org/10.3103/S0003701X17010030.

[9] Solar Paces NREL, CSP Projects Around the World, IEA, Energy Technol. Netw., 2023. https://www.solarpaces.org/csp-technologies/csp-projects-around-the-world/ (accessed June 20, 2023).

[10] A. Calderón, A. Palacios, C. Barreneche, M. Segarra, C. Prieto, A. Rodriguez-Sanchez, A.I. Fernández, High temperature systems using solid particles as TES and HTF material: a review, Appl. Energy 213 (2018) 100–111, https://doi.org/10.1016/j.apenergy.2017.12.107.

[11] IRENA, Innovation outlook: thermal energy storage. https://www.irena.org/publications/2020/Nov/Innovation-outlook-Thermal-energy-storage, 2020.

[12] G. Alva, L. Liu, X. Huang, G. Fang, Thermal energy storage materials and systems for solar energy applications, Renew. Sustain. Energy Rev. 68 (2017) 693–706, https://doi.org/10.1016/j.rser.2016.10.021.

[13] F. Nie, F. Bai, Z. Wang, X. Li, R. Yang, Solid particle solar receivers in the next-generation concentrated solar power plant, EcoMat (2022) 1–27, https://doi.org/10.1002/eom2.12207.

[14] C.S. Turchi, Z. Ma, T.W. Neises, M.J. Wagner, Thermodynamic study of advanced supercritical carbon dioxide power cycles for concentrating solar power systems, J. Sol. Energy Eng. Trans. ASME 135 (2013) 1–7, https://doi.org/10.1115/1.4024030.

[15] C.K. Ho, A review of high-temperature particle receivers for concentrating solar power, Appl. Therm. Eng. 109 (2016) 958–969, https://doi.org/10.1016/j.applthermaleng.2016.04.103.

[16] O. Achkari, A. El fadar, Latest developments on TES and CSP technologies - energy and environmental issues, applications and research trends, Appl. Therm. Eng. 167 (2020), https://doi.org/10.1016/j.applthermaleng.2019.114806.

[17] K. El Alami, M. Asbik, H. Agalit, Identification of natural rocks as storage materials in thermal energy storage (TES) system of concentrated solar power (CSP) plants – a review, Sol. Energy Mater. Sol. Cells 217 (2020) 110599, https://doi.org/10.1016/j.solmat.2020.110599.

[18] K.G. Allen, T.W. Von Backström, D.G. Kröger, A.F.M. Kisters, Rock bed storage for solar thermal power plants: rock characteristics, suitability, and availability, Sol. Energy Mater. Sol. Cells. 126 (2014) 170–183, https://doi.org/10.1016/j.solmat.2014.03.030.

[19] C.K. Ho, Advances in central receivers for concentrating solar applications, Sol. Energy. 152 (2017) 38–56, https://doi.org/10.1016/j.solener.2017.03.048.

[20] J.C. Carracedo, V.R. Troll, J.M.D. Day, H. Geiger, M. Aulinas, V. Soler, F. M. Deegan, F.J. Perez-Torrado, G. Gisbert, E. Gazel, A. Rodriguez-Gonzalez, H. Albert, The 2021 eruption of the cumbre Vieja volcanic ridge on La Palma, Canary Islands, Geol. Today 38 (2022), https://doi.org/10.1111/gto.12388.

[21] S. Gamesa, Volcanic Rock Stores Wind Energy, Fed. Minist. Econ. Aff. Clim., 2019. https://www.bmwi-energiewende.de/EWD/Redaktion/EN/Newsletter/2019/07/Meldung/news2.html (accessed June 29, 2023).

[22] T. Delise, A.C. Tizzoni, M. Ferrara, N. Corsaro, C. D'Ottavi, S. Sau, S. Licoccia, Thermophysical, environmental, and compatibility properties of nitrate and nitrite containing molten salts for medium temperature CSP applications: a critical review, J. Eur. Ceram. Soc. 39 (2019) 92–99, https://doi.org/10.1016/j.jeurceramsoc.2018.07.057.

[23] A. Svobodova-Sedlackova, S. Huete-Hernández, A. Calderón, C. Barreneche, P. Gamallo, A.I. Fernandez, Effect of nanoparticles on the thermal stability and reaction kinetics in ionic nanofluids, Nanomaterials 12 (2022), https://doi.org/10.3390/nano12101777.

[24] G. Ferrer, C. Barreneche, A. Solé, I. Martorell, L.F. Cabeza, New proposed methodology for specific heat capacity determination of materials for thermal energy storage (TES) by DSC, J. Energy Storage 11 (2017) 1–6, https://doi.org/10.1016/j.est.2017.02.002.

[25] F. Sutter, M. Montecchi, A. Morales, G. San Vicente, A. Fernandez-Garcia, J. Pernpeintner, J.T. Reche-Navarro, L. Martinez-Arcos, J. Wette, A. Calderon, M. Majó, A.I. Fernández, P. Davenport, T. Farrell, C. Ho, Round robin test of absorptance and emittance of particles for CSP, in: AIP Publ. 26th SolarPACES Conf, 2022. https://elib.dlr.de/189589/.

[26] A. Palacios, A. Calderón, C. Barreneche, J. Bertomeu, M. Segarra, A.I. Fernández, Study on solar absorptance and thermal stability of solid particles materials used as TES at high temperature on di ff erent aging stages for CSP applications, Sol. Energy Mater. Sol. Cells 201 (2019) 110088, https://doi.org/10.1016/j.solmat.2019.110088.

[27] A. White, J. McTigue, C. Markides, Wave propagation and thermodynamic losses in packed-bed thermal reservoirs for energy storage, Appl. Energy 130 (2014) 648–657, https://doi.org/10.1016/j.apenergy.2014.02.071.

[28] J. Mañosa, J. Serrano-Conte, A. Maldonado-Alameda, M. Aulinas, J.M. Chimenos, Pyroclastic volcanic ash as a potential precursor of alkali-activated binders – a case study from Tajogaite (La Palma, Canary Islands) volcano eruption, Build. Eng. 72 (2023), https://doi.org/10.1016/j.jobe.2023.106623.

[29] J.M.D. Day, H. Geiger, V.R. Troll, F.J. Perez-torrado, M. Aulinas, G. Gisbert, J. C. Carracedo, Bouncing spallation bombs during the 2021 La Palma eruption, Canary Islands, Spain, Earth Sci. Syst. Soc. 2 (2022) 1–9, https://doi.org/10.3389/esss.2022.10063.

[30] J. Mazo-Zuluaga, C.A. Barrero, J. Díaz-Terán, A. Jerez, Thermally induced magnetite-haematite transformation, Hyperfine Interact. 148–149 (2003) 153–161, https://doi.org/10.1023/B:HYPE.0000003776.84005.89.

[31] E.A. Gorbatova, V.V. Kholodnov, B.I. Pirogov, M.S. Kolkova, E.S. Shagalov, Solid-phase transformations of titanomagnetite and ilmenite during oxidizing roasting of disseminated titanomagnetite–ilmenite ore at the Medvedevskoe deposit and certain geological events (Southern Urals), Geol. Ore Depos. 63 (2021) 431–453, https://doi.org/10.1134/S1075701521040036.

[32] C. Villada, A. Bonk, T. Bauer, F. Bolívar, High-temperature stability of nitrate/nitrite molten salt mixtures under different atmospheres, Appl. Energy 226 (2018) 107–115, https://doi.org/10.1016/j.apenergy.2018.05.101.

[33] A. Lomonaco, D. Haillot, E. Pernot, E. Franquet, J.P. Bédécarrats, Sodium nitrate thermal behavior in latent heat thermal energy storage: a study of the impact of sodium nitrite on melting temperature and enthalpy, Sol. Energy Mater. Sol. Cells. 149 (2016) 81–87, https://doi.org/10.1016/j.solmat.2015.12.043.

[34] A. Lomonaco, D. Haillot, E. Pernot, E. Franquet, A. Lomonaco, D. Haillot, E. Pernot, E. Franquet, J.B. Thermal, A. Lomonaco, D. Haillot, E. Pernot, E. Franquet, Thermal characterization of sodium nitrate-sodium nitrite compounds for thermal storage applications, in: ECOS 2015 - 28th Int. Conf. Effic. Cost, Optim. Simul. Environ- Ment. Impact Energy Syst, 2019.

[35] C. Zhang, Y. Han, Y. Wu, Y. Lu, Comparative study on high temperature thermal stability of quaternary nitrate-nitrite mixed salt and Solar salt, Sol. Energy Mater. Sol. Cells. 230 (2021) 111197, https://doi.org/10.1016/j.solmat.2021.111197.

[36] P.D. Desai, C.Y. Ho, Thermal Linear Expansion of Nine Selected AISI Stainless Steels 51, Am. Iron Steel Inst., 1978. https://apps.dtic.mil/sti/citations/ADA129159.

[37] S. Raju, K. Sivasubramanian, R. Divakar, G. Panneerselvam, A. Banerjee, E. Mohandas, M.P. Antony, Thermal expansion studies on Inconel-600® by high temperature X-ray diffraction, J. Nucl. Mater. 325 (2004) 18–25, https://doi.org/10.1016/j.jnucmat.2003.10.007.

[38] A. Calderón, C. Barreneche, A.I. Fernández, M. Segarra, Thermal cycling test of solid particles to be used in concentrating solar power plants, Sol. Energy Mater. Sol. Cells. 222 (2021), https://doi.org/10.1016/j.solmat.2020.110936.